Chemical Engineering Journal xxx (xxxx) xxx–xxx

Contents lists available at ScienceDirect

Chemical Engineering Journal

journal homepage: www.elsevier.com/locate/cej

Multi-scale CFD simulations of bubbling fluidized bed methanation process

Jiageng Li, Bolun Yang*

Department of Chemical Engineering, State Key Laboratory of Multiphase Flow in Power Engineering, Xi'an Jiaotong University, Xi'an, Shaanxi 710049, PR China

HIGHLIGHTS

- A multi-scale CFD model for the fluidized bed methanation process is established.
- The multi-scale model is validated by the experiments under different operating conditions.
- The effects of the methanation reactions on the meso-scale structure is studied.
- The isothermal flow assumption for the simulation of the fluidized bed methanation is verified.

ARTICLE INFO

Keywords:
Multi-scale
CFD simulation
Fluidized bed
Methanation
Meso-scale structure

ABSTRACT

The two-fluid model coupled with the improved local-structure-dependent drag model and the modified chemical kinetics is employed to account for the multi-scale phenomenon in a bubbling fluidized bed methanation process for the production of synthetic natural gas. The accuracy of this multi-scale CFD model is verified by a series of experimental data under different operating temperatures, inlet compositions, inlet velocities and initial bed heights. The cold flow CFD simulations are further carried out to evaluate the effects of the chemical reactions on the meso-scale structure. The results demonstrate that the bubble volume fraction and bubble velocity decreases due to the gas volume contraction caused by the methanation reactions. Three-region distribution of the gas temperature is obtained by simultaneously solving the multi-scale CFD model and the energy equations and the simulation results are compared with those based on the isothermal flow assumption. The results indicate that the distributions of solid volume fraction and mole fractions obtained based on the isothermal flow assumption are almost coincident with those obtained by solving the energy equations, which confirms the rationality of the isothermal flow assumption in a fluidized bed reactor.

1. Introduction

Bubbling fluidized bed reactors are widely used in the chemical industry due to their good heat and mass transfer performance as well as their ease of operation and control, particularly in highly exothermic chemical processes such as methanation of coal, biomass and coke oven gas to produce synthetic natural gas (SNG) [1–4]. Compared with experimental research, numerical simulations can improve the efficiency of the design, scale-up and optimization of a reactor because the steps of the machining and fabrication can be reduced, and can also study under extreme conditions [5,6].

However, the feature of multi-scale structure existing in the fluidized bed methanation system increases the complexity of the numerical simulation and affects the accuracy of the simulation results [7–9]. In the entire reactor scale (macro-scale), the distributions of catalyst particles and gas velocity, as well as the mixing of solid particles and backmixing of the gas phase determine the overall performance of the reactor. In the catalyst particle scale (micro-scale), changes in the concentrations and temperature caused by the chemical reactions affect the macroscopic physical properties of the gas phase, which further influences the flow structure in the macro-scale. Between the reactor and the single catalyst particle, the gas and solid phases are respectively agglomerated to form the meso-scale structure characterized by bubbles [10–12]. The coalescence and breakup of the bubbles affect the mixing of the particles and backmixing of the gas phase in the entire reactor. Thus, there are complex interactions between the scales in the fluidized bed methanation system. How to numerically describe the physical and chemical processes within each scale and reasonably couple the different scales are the key to accurate simulation of the methanation process and further realization of the design and scale-up of the fluidized bed.

At present, the two-fluid model (TFM) based on the Eulerian-

* Corresponding author.
E-mail address: blunyang@mail.xjtu.edu.cn (B. Yang).

https://doi.org/10.1016/j.cej.2018.08.204

Nomenclature

a	acceleration ($m{\cdot}s^{-2}$)
C_{D0}	drag coefficient of a single particle (−)
d_p	diameter of catalyst particle (m)
E_A	activation energy ($J{\cdot}mol^{-1}$)
e	restitution coefficient (−)
F_{drag}	drag force per unit volume ($N{\cdot}m^{-3}$)
$\boldsymbol{g}$	gravitational acceleration ($m{\cdot}s^{-2}$)
g_0	radial distribution function (−)
H	specific enthalpy ($J{\cdot}kg^{-1}$)
H_{exp}	bed expansion height (m)
H_d	heterogeneity index (−)
h	interphase heat transfer coefficient ($W{\cdot}m^{-3}{\cdot}K^{-1}$)
$\boldsymbol{I}$	unit tensor (−)
$\boldsymbol{J}_i$	diffusion flux of species i ($kg{\cdot}m^{-2}{\cdot}s^{-1}$)
K_C, K_{OH}	adsorption equilibrium constants ($bar^{-0.5}$)
K_j	equilibrium constants of reaction j, j = METH, WGS ($bar^{\Sigma\nu}$)
k_{METH}	METH reaction rate constant ($mol{\cdot}s^{-1}{\cdot}kg_{cat}{}^{-1}{\cdot}bar^{-0.5}$)
k_{WGS}	WGS reaction rate constant ($mol{\cdot}s^{-1}{\cdot}kg_{cat}{}^{-1}{\cdot}bar^{-1.5}$)
k_Θ	diffusion coefficient for granular energy ($kg{\cdot}m^{-1}{\cdot}s^{-1}$)
M_i	mole weight of species i ($kg{\cdot}mol^{-1}$)
Nu_p	particle Nusselt number (−)
N_s	suspension energy consumption rates ($J{\cdot}s^{-1}{\cdot}kg^{-1}$)
P_{op}	operating pressure (Pa)
P	gauge pressure (Pa)
p_i	partial pressure of species i (bar)
R	ideal gas constant ($J{\cdot}mol^{-1}{\cdot}K^{-1}$)
R_i	reaction rate of species i ($kg{\cdot}m^{-3}{\cdot}s^{-1}$)
r_j	reaction rate of reaction j, j = METH, WGS ($mol{\cdot}kg_{cat}{}^{-1}{\cdot}s^{-1}$)
Re_p	particle Reynolds number (−)
S	heat source ($W{\cdot}m^{-3}$)
T	temperature (K)
$\boldsymbol{U}$	velocity ($m{\cdot}s^{-1}$)
u_{slip}	superficial slip velocity ($m{\cdot}s^{-1}$)
Y_i	mass fraction of species i (−)

Greek symbols

β	drag coefficient ($kg{\cdot}m^{-3}{\cdot}s^{-1}$)
ΔH_j	reaction enthalpy of reaction j ($J{\cdot}mol^{-1}$)
γ_Θ	collisional dissipation of granular energy ($kg{\cdot}m^{-1}{\cdot}s^{-3}$)
δ_b	bubble volume fraction (−)
ε	phase volume fraction (−)
ε_b	voidage of the bubble phase (−)
ε_e	voidage of the emulsion phase (−)
Θ	granular temperature ($m^2{\cdot}s^{-2}$)
κ	thermal conductivity ($W{\cdot}m^{-1}{\cdot}K^{-1}$)
λ_p	bulk viscosity of particle phase (Pa·s)
μ	viscosity (Pa·s)
$\nu_{j,i}$	stoichiometric coefficients of species i in reaction j (−)
ρ	density ($kg{\cdot}m^{-3}$)
τ	Stress-strain tensor (Pa)
φ_{gp}	interphase energy exchange ($kg{\cdot}m^{-1}{\cdot}s^{-3}$)
φ_k	switching functions, $k = L, U$ (−)

Subscripts

g	gas phase
i	CO, H_2, CH_4, CO_2, H_2O, Ar
METH	CO methanation reaction
p	particle phase
WGS	water-gas shift reaction

Eulerian point of view is widely applied in the simulation of gas-solid two-phase flow because of its low computational resource consumption [13,14]. By simultaneously solving the TFM, the species transport equations and energy equations, the macro-scale variables such as gas and solid velocities, solid volume fraction, pressure, concentrations of all the components and temperature can be obtained. The existence of heterogeneous meso-scale structure results in the gas–solid drag force in the macroscopic momentum equations being smaller than the drag force calculated by the conventional drag models [15], which leads to different distributions of gas–solid velocity, solid volume fraction and pressure. The consumption and generation of each species on the micro-scale catalyst particle, and the release of reaction heat will cause changes in the source terms of the macro-scale species transport equations and the energy equations, thereby affecting the distribution of the concentrations and temperature in a reactor. Therefore, the accuracy of the meso-scale model and micro-scale model is a crucial factor in predicting the performance of a reactor.

In recent years, many researchers have applied computational fluid dynamics (CFD) simulation methods to predict the transfer phenomena and chemical reactions in fluidized bed reactors, which provides new ideas and tools for the study of fluidized bed reactors. Zhao et al. [16] studied the methanol to olefins (MTO) process in a fluidized bed reactor. The results showed that the energy-minimized multi-scale (EMMS) drag model can provide more accurate distribution of solid volume fraction than the conventional Gidaspow drag model because the effects of the meso-scale structure were considered in the EMMS model. The selectivity of the main products at the reactor outlet was also well predicted. Salehi et al. [17] investigated the effects of operating conditions and feed characteristics on the performance of a fluidized bed reactor for the oxidation coupling of methane (OCM) process. The simulation results were also in agreement well with the experimental data.

Numerical simulations of the fluidized bed methanation process have also been performed in some work. Liu and Hinrichsen [18] developed a CFD solver based on the open source package OpenFOAM to simulate the fluidized bed methanation process. The effects of inlet gas velocity, inlet composition and catalyst inventory on reactor performance were studied. Isothermal flow assumption was used in their simulations and therefore the energy equations were not solved. Although the fluidized bed reactor has good heat transfer performance and the bed temperature distribution is relatively uniform, the highly exothermic methanation reactions may cause non-uniformity of the bed temperature. Thus, the rationality of the isothermal flow assumption needs further verification. Sun et al. [19] used the open source package MFiX to simulate the fluidized bed methanation process, and considered the influence of particle cluster on the chemical reactions, and further analyzed the effects of different operating conditions on the performance of the reactor. In the above mentioned simulation work of fluidized bed methanation, the chemical reactions in the micro-scale did not consider the limitation of chemical equilibrium, so the simulations were performed at only single temperature of 320 °C and could not be extended to a wider temperature range.

In the existing numerical simulations of the fluidized bed methanation process, the micro-scale reaction kinetics cannot be applied to higher temperature and thus the dynamic simulation of the methanation system is limited; the effect of the meso-scale structure on the drag model is seldom considered; the influence of gas volume contraction caused by mole-number-reduced methanation reactions on the mesoscopic flow structure has not been investigated yet; whether the isothermal flow assumption is suitable for the simulation of the highly

exothermic fluidized bed methanation process still needs to be further confirmed.

Aiming at these problems, in this work, the modified kinetic model of Kopyscinski et al. [20] is applied to calculate the reaction rates in the micro-scale so that the applicability of the numerical model at higher temperature is ensured. The original local-structure-dependent (LSD) drag model in our pervious study [21] is improved by introducing two switching functions to smooth the piecewise functions of the drag coefficient; this improved LSD drag model is employed in this study to account for the effect of meso-scale structure on the drag model and also to guarantee the convergence of the continuity equations and the momentum equations. Then, the micro-scale reaction kinetic model, the meso-scale heterogeneous drag model and the macro-scale model are coupled to simulate the gas–solid two-phase flow, heat transfer, mass transfer and chemical reactions in the fluidized bed methanation process. The accuracy and the application scope of the multi-scale CFD model are verified by a series of experimental data obtained under different temperatures, inlet compositions, inlet gas velocities and initial bed height. Furthermore, the influence of gas volume contraction caused by micro-scale chemical reactions on the mesoscopic flow structures is further studied, which provides a basis for the development of the meso-scale drag model. Finally, the rationality of the isothermal flow assumption for the simulation of the highly exothermal fluidized bed methanation process is discussed.

2. Multi-scale model

2.1. Macro-scale model

2.1.1. Governing equations

2.1.1.1. Continuity equations. In a fluidized bed methanation reactor, the continuity equations for the gas and particle phase are

$$\frac{\partial}{\partial t}(\varepsilon_g\rho_g) + \nabla\cdot(\varepsilon_g\rho_g\boldsymbol{u}_g) = 0 \tag{1}$$

$$\frac{\partial}{\partial t}(\varepsilon_p\rho_p) + \nabla\cdot(\varepsilon_p\rho_p\boldsymbol{u}_p) = 0 \tag{2}$$

where ε, ρ and $\boldsymbol{u}$ are phase volume fraction, density and velocity, respectively. Chemical reactions in the methanation system only occur in the gas phase, which cannot lead to extra mass source in two phases. Thus, the right-hand of the continuity equations are both zero. The gas density (ρ_g) in the gas continuity equation is a function of gas composition and gas temperature, and can be calculated using compressible ideal gas state equation:

$$\rho_g = \frac{P_{op} + p}{RT_g\sum_i \frac{Y_i}{M_i}} \tag{3}$$

In Eq. (3) P_{op}, p, R, T_g, Y_i and M_i are the operating pressure, gauge pressure, ideal gas constant, gas temperature, mass fraction of species i and mole weight of species i, respectively.

2.1.1.2. Momentum equations. The momentum equations for the gas and solid phase can be written as

$$\frac{\partial}{\partial t}(\varepsilon_g\rho_g\boldsymbol{u}_g) + \nabla\cdot(\varepsilon_g\rho_g\boldsymbol{u}_g\boldsymbol{u}_g) = -\varepsilon_g\nabla p + \nabla\cdot\boldsymbol{\tau}_g + \varepsilon_g\rho_g\boldsymbol{g} - \beta(\boldsymbol{u}_g - \boldsymbol{u}_p) \tag{4}$$

$$\frac{\partial}{\partial t}(\varepsilon_p\rho_p\boldsymbol{u}_p) + \nabla\cdot(\varepsilon_p\rho_p\boldsymbol{u}_p\boldsymbol{u}_p) = -\varepsilon_p\nabla p - \nabla p_p + \nabla\cdot\boldsymbol{\tau}_p + \varepsilon_p\rho_p\boldsymbol{g} - \beta(\boldsymbol{u}_p - \boldsymbol{u}_g) \tag{5}$$

where τ, $\boldsymbol{g}$ and are stress–strain tensor, gravitational acceleration and interphase drag coefficient, respectively. Constitutive equations are used to calculate τ and meso-scale model will develop to calculate .

2.1.1.3. Gas species transport equations. The gas species transport equation for species i in the gas phase is

$$\frac{\partial}{\partial t}(\varepsilon_g\rho_g Y_i) + \nabla\cdot(\varepsilon_g\rho_g\boldsymbol{u}_g Y_i) = -\nabla\cdot(\varepsilon_g\boldsymbol{J}_i) + R_i \tag{6}$$

where $\boldsymbol{J}_i$ is the diffusion flux of species i and can be expressed as Eq. (7), and R_i is the generating rate of species i due to chemical reactions.

$$\boldsymbol{J}_i = -\rho_g D_{i,m}\nabla Y_i \tag{7}$$

2.1.1.4. Energy equations. The energy equations for the gas phase and particle phase are

$$\frac{\partial}{\partial t}(\varepsilon_g\rho_g H_g) + \nabla\cdot(\varepsilon_g\rho_g\boldsymbol{u}_g H_g) = \nabla(\kappa_g\nabla T_g) + h(T_g - T_p) + S_g \tag{8}$$

$$\frac{\partial}{\partial t}(\varepsilon_p\rho_p H_p) + \nabla\cdot(\varepsilon_p\rho_p\boldsymbol{u}_p H_p) = \nabla(\kappa_p\nabla T_p) + h(T_p - T_g) + S_p \tag{9}$$

where H, κ, T and S are specific enthalpy, thermal conductivity, temperature and heat source due to chemical reactions, respectively. h is the interphase heat transfer coefficient and can be calculated by

$$h = \frac{6k_g\varepsilon_g\varepsilon_p\mathrm{Nu}_p}{d_p^2} \tag{10}$$

where Nu_p is the particle Nusselt number and can be derived by the correlation of Gunn [22]:

$$\mathrm{Nu}_p = (7-10\varepsilon_g + 5\varepsilon_g^2)(1 + 0.7\mathrm{Re}_p^{0.2}\mathrm{Pr}^{1/3}) + (1.33-2.4\varepsilon_g + 1.2\varepsilon_g^2)\mathrm{Re}_p^{0.7}\mathrm{Pr}^{1/3} \tag{11}$$

2.1.2. Constitutive equations

The stress–strain tensors in the momentum equations can be given as

$$\boldsymbol{\tau}_g = \varepsilon_g\mu_g[\nabla\boldsymbol{u}_g + (\nabla\boldsymbol{u}_g)^{\mathrm{T}}] - \frac{2}{3}\varepsilon_g\mu_g\nabla\boldsymbol{u}_g\boldsymbol{I} \tag{12}$$

$$\boldsymbol{\tau}_p = \varepsilon_p\mu_p[\nabla\boldsymbol{u}_p + (\nabla\boldsymbol{u}_p)^{\mathrm{T}}] + \varepsilon_p(\lambda_p - \frac{2}{3}\mu_p)\nabla\boldsymbol{u}_p\boldsymbol{I} \tag{13}$$

where μ is the shear viscosity, λ_p is the bulk viscosity of particle phase and $\boldsymbol{I}$ is the unit tensor. μ_g can be obtained by mass-weighted mixing rule:

$$\mu_g = \sum_i Y_i\mu_{g,i} \tag{14}$$

where the shear viscosity of species i, $\mu_{g,i}$, is determined according to Sutherland's law:

$$\mu_{g,i} = \mu_{g,i}^0(\frac{T_g}{T_{0,i}})^{3/2}\frac{T_{0,i} + S_i}{T_g + S_i} \tag{15}$$

p_p, μ_p and λ_p in Eqs. (5) and (13) are solved using the kinetic theory of granular flow (KTGF) and can be eventually expressed as the functions of granular temperature (Θ). The transport equation for the calculation of Θ takes the form:

$$\frac{3}{2}[\frac{\partial}{\partial t}(\rho_p\varepsilon_p\Theta) + \nabla\cdot(\rho_p\varepsilon_p\boldsymbol{u}_p\Theta)] = (-p_p\boldsymbol{I} + \boldsymbol{\tau}_p)\colon\nabla\boldsymbol{u}_p + \nabla\cdot(k_\Theta\nabla\Theta) - \gamma_\Theta + \phi_{gp} \tag{16}$$

The first two terms on the right-hand side of Eq. (16) represent the generation of granular energy due to solid stress and diffusion, respectively. k_Θ is the diffusion coefficient for granular energy and is given by

$$k_\Theta = \frac{15d_p\rho_p\varepsilon_p\sqrt{\Theta\pi}}{2(49-33e)}[1 + \frac{3}{5}(1+e)^2(2e-1)\varepsilon_p g_0 + \frac{4}{15\pi}(49-33e)(1+e)\varepsilon_p g_0] \tag{17}$$

where e is restitution coefficient for particle collisions, and the radial distribution function, g_0, is expressed as

$$g_0 = [1-(\varepsilon_p/\varepsilon_{p,\max})^{1/3}]^{-1} \quad (18)$$

γ_Θ in Eq. (16) is collisional dissipation of granular energy and is obtained by

$$\gamma_\Theta = 12(1-e^2)\frac{\rho_p \varepsilon_p^2 g_0}{d_p\sqrt{\pi}}\Theta^{3/2} \quad (19)$$

ϕ_{gp} in Eq. (16) is interphase energy exchange and is calculated by

$$\phi_{gp} = -3\beta\ \Theta \quad (20)$$

Then, p_p, μ_p and $_p$ can be written as

$$p_p = [1 + 2\rho_p(1+e)\varepsilon_p]\varepsilon_p g_0 \Theta \quad (21)$$

$$\mu_p = \frac{4}{5}\varepsilon_p\rho_p d_p g_0(1+e)\sqrt{\frac{\Theta}{\pi}} + \frac{\varepsilon_p d_p \rho_p\sqrt{\Theta\pi}}{6(3-e)}[1+\frac{2}{5}(1+e)(3e-1)\varepsilon_p g_0] + \frac{p_p \sin\varphi}{2\sqrt{I_{2D}}} \quad (22)$$

$$\lambda_p = \frac{4}{3}\varepsilon_p^2\rho_p d_p g_0(1+e)\sqrt{\frac{\Theta}{\pi}} \quad (23)$$

2.2. Meso-scale model

Meso-scale model is developed to account for the influence of heterogeneous flow structure on the gas–solid interactions. In this study, a local-structure-dependent (LSD) model established in our previous study [21] is improved and employed to calculate the drag force. Based on the original LSD drag model, two switching functions are introduced to smooth of the drag force function, which can improve the convergence of the continuity equations and the momentum equations in the CFD model. The model equations are detailed in Table 1.
The heterogeneous drag coefficient is eventually obtained as

$$\beta = (1-\varphi_L)(1-\varphi_U)\beta_{\text{Ergun}} + \varphi_L(1-\varphi_U)\beta_{\text{LSD}} + \varphi_L\varphi_U\beta_{\text{Wen \& Yu}} \quad (24)$$

where β_{Ergun}, β_{LSD} and $\beta_{\text{Wen\&Yu}}$ are the drag coefficients calculated by the models of Ergun, LSD and Wen & Yu, respectively, and they are expressed as

$$\beta_{\text{Ergun}} = 150\frac{(1-\varepsilon_g)^2\mu_g}{\varepsilon_g d_p^2} + 1.75(1-\varepsilon_g)\frac{\rho_g}{d_p}|\boldsymbol{u}_g-\boldsymbol{u}_p| \quad (25)$$

$$\beta_{\text{LSD}} = \frac{3}{4}C_{D0}\frac{(1-\varepsilon_g)\varepsilon_g\rho_g|\boldsymbol{u}_g-\boldsymbol{u}_p|}{d_p}\varepsilon_g^{-2.65}\cdot H_d \quad (26)$$

$$\beta_{\text{Wen \& Yu}} = \frac{3}{4}C_{D0}\frac{(1-\varepsilon_g)\varepsilon_g\rho_g|\boldsymbol{u}_g-\boldsymbol{u}_p|}{d_p}\varepsilon_g^{-2.65} \quad (27)$$

where H_d is the heterogeneity index calculated by LSD drag model for this gas–solid system

$$H_d = \exp[-0.007473(\ln \text{Re}_p)^2 - 1.075\ln \text{Re}_p - 0.8392]\varepsilon_g^{4.646} \quad (28)$$

The switching functions (φ) at lower and upper boundaries in Eq. (24) have the form

$$\varphi_k = \frac{1}{2} + \frac{\arctan[50(\varepsilon_g-\varepsilon_{gk})]}{\pi} \quad k = L,\ U \quad (29)$$

where the ε_{gL} and ε_{gU} can be calculated by

$$\varepsilon_{gL} = \begin{cases} 0.45 & \text{Re}_p \leqslant 0.03596 \\ 1.402\text{Re}_p^{0.2273} - 0.2084 & 0.03596 < \text{Re}_p \leqslant 0.5005 \\ 0.9895 & \text{Re}_p > 0.5005 \end{cases} \quad (30)$$

$$\varepsilon_{gU} = \begin{cases} 9.205\text{Re}_p + 0.45 & \text{Re}_p \leqslant 0.01545 \\ 1.689\text{Re}_p^{0.1739} - 0.2350 & 0.01545 < \text{Re}_p \leqslant 0.1653 \\ 1.0 & \text{Re}_p > 0.1653 \end{cases} \quad (31)$$

2.3. Micro-scale model

In the micro-scale catalyst particle, chemical reactions including CO methanation (METH) and water–gas shift (WGS) reaction occur.

$$\text{CO} + 3\text{H}_2 \rightleftharpoons \text{CH}_4 + \text{H}_2\text{O} \quad \Delta H_{298\text{K}} = -206.28\ \text{kJ·mol}^{-1} \quad (32)$$

$$\text{CO} + \text{H}_2\text{O} \rightleftharpoons \text{CO}_2 + \text{H}_2 \quad \Delta H_{298\text{K}} = -41.46\ \text{kJ·mol}^{-1} \quad (33)$$

The kinetic model of Kopyscinski et al [20] is frequently used in the simulation work about methanation [18,19,23]. However, this model is available only at low temperature (< 400 °C) because the chemical equilibrium is not considered in the rate expression of the CO methanation. Here, a modified kinetic model based on the model of Kopyscinski et al. [20] is adopted to calculate the reaction rates.

$$r_{\text{METH}} = \frac{k_{\text{METH}}K_{\text{C}}\left(p_{\text{CO}}p_{\text{H}_2}^3 - p_{\text{CH}_4}p_{\text{H}_2\text{O}}/K_{\text{METH}}\right)}{p_{\text{CO}}^{0.5}p_{\text{H}_2}^{2.5}\left(1+K_{\text{C}}p_{\text{CO}}^{0.5}+K_{\text{OH}}p_{\text{H}_2\text{O}}p_{\text{H}_2}^{-0.5}\right)^2} \quad \frac{\text{mol}}{\text{kg}_{\text{cat}}\cdot\text{s}} \quad (34)$$

$$r_{\text{WGS}} = \frac{k_{\text{WGS}}\left(p_{\text{CO}}p_{\text{H}_2\text{O}} - p_{\text{CO}_2}p_{\text{H}_2}/K_{\text{WGS}}\right)}{p_{\text{H}_2}^{0.5}\left(1+K_{\text{C}}p_{\text{CO}}^{0.5}+K_{\text{OH}}p_{\text{H}_2\text{O}}p_{\text{H}_2}^{-0.5}\right)^2} \quad \frac{\text{mol}}{\text{kg}_{\text{cat}}\cdot\text{s}} \quad (35)$$

This modified kinetic model has been verified to provide accurate reaction rate at wide temperature range for the CO methanation process in our previous study [24]. The reaction rate constants, equilibrium constants and the adsorption equilibrium constants in Eqs. (34) and (35) can be formulated as

$$k_j = k_{j,T_{ref}}\exp[\tfrac{E_{A,j}}{RT_{ref}}(1-\tfrac{T_{ref}}{T_g})] \quad (j = \text{METH,WGS}) \quad (36)$$

$$K_j = K_{j,T_{ref}}\exp[\tfrac{\Delta H_j}{RT_{ref}}(1-\tfrac{T_{ref}}{T_g})] \quad (j = \text{METH, WGS, C,OH}) \quad (37)$$

where the relevant parameters can be found in Table 2.
The reaction enthalpies of the two reactions are:

$$\Delta H_{\text{METH}} = -189283 - 64.4338T_g + 0.0297292T_g^2 - 1.36306\times10^{-6}T_g^3 \quad (\text{J·mol}^{-1}) \quad (38)$$

$$\Delta H_{\text{WGS}} = -40821.1 - 7.55185T_g + 0.0236384T_g^2 - 1.02182\times10^{-5}T_g^3 \quad (\text{J·mol}^{-1}) \quad (39)$$

Therefore, R_i in species transport equations (Eq. (6)) can be calculated as

$$R_i = \rho_p\varepsilon_p M_i(\nu_{\text{METH},i}r_{\text{METH}} + \nu_{\text{WGS},i}r_{\text{WGS}}) \quad (40)$$

Table 1
LSD drag model.

Particle force balance in the emulsion phase: $(1-\delta_b)F_{drag,e} + F_{drag,i} \approx (1-\delta_b)(1-\varepsilon_e)(\rho_p-\rho_g)(g+a_{pe})$
Particle force balance in the bubble phase: $\delta_b F_{drag,b} \approx \delta_b(1-\varepsilon_b)(\rho_p-\rho_g)(g+a_{pb})$
Particle force balance in the inter phase: $F_{drag,i} \approx (\varepsilon_g-\varepsilon_e)(\rho_p-\rho_g)(g-a_b)$
Gas force balance: $F_{drag,e} = F_{drag,b} + \frac{F_{drag,i}}{\delta_b}$
Correlation of slip velocities: $u_{slip,i} = \frac{\varepsilon_b(1-\varepsilon_e)(1-\varepsilon_g)}{\varepsilon_g-\varepsilon_e}[u_{slip}-(1-\delta_b)u_{slip,e}-\frac{\delta_b\varepsilon_g(1-\varepsilon_b)}{\varepsilon_b(1-\varepsilon_g)}u_{slip,b}]$
Voidage equation: $\varepsilon_g = (1-\delta_b)\varepsilon_e + \delta_b\varepsilon_b$
Stability condition: $N_s = \frac{(1-\delta_b)F_{drag,e}\cdot u_{ge} + \delta_b F_{drag,b}\cdot u_{gb} + F_{drag,i}\cdot u_{gb}\delta_b}{(1-\varepsilon_g)\rho_p} \rightarrow \min$
Heterogeneous drag force: $\beta_{LSD} = \frac{\varepsilon_g^2}{u_{slip}}[(1-\delta_b)F_{drag,e} + \delta_b F_{drag,b} + F_{drag,i}]$

Table 2
Kinetic parameters used in this study.

k_j or K_j	$k_{j,Tref}$ or $K_{j\ Tref}$	$E_{A,j}$ or ΔH_j
k_{METH}	1.16 $mol{\cdot}s^{-1}{\cdot}kg_{cat}{}^{-1}{\cdot}bar^{-0.5}$	74.1 $kJ{\cdot}mol^{-1}$
k_{WGS}	2.43 $mol{\cdot}s^{-1}{\cdot}kg_{cat}{}^{-1}{\cdot}bar^{-1.5}$	154.2 $kJ{\cdot}mol^{-1}$
K_{METH}	2.52×10^6 bar^{-2}	−223.1 $kJ{\cdot}mol^{-1}$
K_{WGS}	29.2	−38.94 $kJ{\cdot}mol^{-1}$
K_C	1.77 $bar^{-0.5}$	−61.0 $kJ{\cdot}mol^{-1}$
K_{OH}	0.66 $bar^{-0.5}$	−72.3 $kJ{\cdot}mol^{-1}$

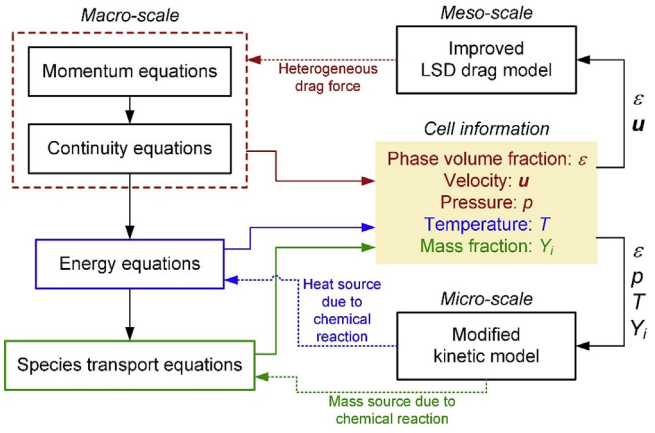

Fig. 1. Coupling of the multi-scale CFD model in a computational cell.

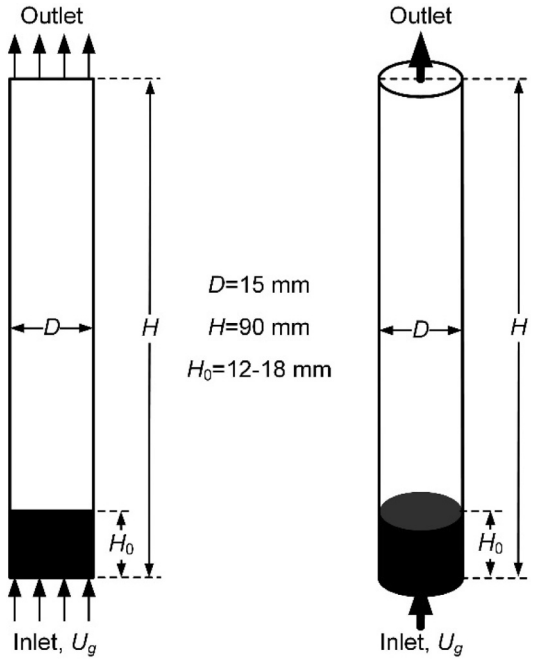

Fig. 2. Geometries of the lab-scale bubbling fluidized bed for 2D and 3D simulations.

where $\nu_{METH,i}$ and $\nu_{WGS,i}$ are the stoichiometric coefficients of species i in the CO methanation and water–gas shift reaction, respectively. Heat source due to chemical reactions in the energy equations (S_g and S_p) can be written as

$$S_g = \rho_p \varepsilon_p (\Delta H_{METH} r_{METH} + \Delta H_{METH} r_{WGS}) \quad (41)$$

$$S_p = 0 \quad (42)$$

Table 3
simulation parameters setup.

Parameters	Value
Operating temperature (°C)	350, 400, 450, 500
Inlet composition (y_{CO}:y_{H2}:y_{Ar})	1:7:2, 1.5:6.5:2, 2:6:2, 2.5:5.5:2, 3:5:2
Inlet velocity ($m{\cdot}s^{-1}$)	0.108, 0.162, 0.216, 0.270, 0.324
Initial bed height (mm)	12, 15, 18
Operating pressure (Pa)	101325
Pressure-velocity coupling	Phase coupled SIMPLE
Momentum discretization	Second order upwind
Volume fraction discretization	QUICK
Granular Temperature discretization	Second order upwind
Energy discretization	Second order upwind
Gas species discretization	Second order upwind
Convergence criteria	10^{-3}
Time step (s)	< 0.0005

2.4. Coupling of the multi-scale model

The coupling of the multi-scale model is shown in Fig. 1. In a computational cell, the macro-scale model is solved by using the CFD solver and the cell information including the parameters of phase volume fraction (ε), velocity ($\boldsymbol{u}$), pressure (p), temperature (T) and mass fraction (Y_i) is obtained. Then, the cell information is used as the input of the meso-scale model and micro-scale model to calculate the heterogeneous drag force and heat and mass source due to chemical reactions, respectively. The drag force, heat source and mass source are then substituted into the momentum equations, energy equations and the species transport equations, respectively. The macro-scale model is solved again to obtained the new cell information. This process continues proceeding until the parameters in a computational cell are converged.

3. Simulation setup

In this study, CFD simulations are based on a lab-scale bubbling fluidized bed reactor in our previous experimental studies [24] to validate this multi-scale CFD model. The 2D and 3D geometries for the reactor are shown in Fig. 2. The inlet gas is the mixture of CO, H_2 and Ar with different inlet velocities and compositions. The particle phase in the simulations is the Ni-based catalyst with the density of 1684 $kg{\cdot}m^{-3}$ and the diameter of 125 μm. The grid sizes of 1.5 mm (coarse), 0.75 mm (medium) and 0.5 mm (fine) are used for 2D and 3D simulations to test the grid independence. The meshed geometries are imported into FLUENT software to simulate the fluidized bed methanation process. The detail simulation parameters are listed in Table 3. Time statistics for all the simulations last for 5 s in physical time after the gas–solid flow structure are fully developed. Then, the time-averaged results are compared with the experimental data to verify the CFD simulations.

4. Results and discussion

4.1. Grid independence

The axial distributions of time-averaged solid volume fraction, CH_4 mole fraction and CO_2 mole fraction as well as the instantaneous contours of the solid volume fraction and CO_2 mole fraction are displayed in Fig. 3 to illustrate the grid independence. It can be found that the grid independence is achieved at medium grid for both 2D and 3D simulations. There are significant differences between the results of coarse grid simulation and those of medium and fine grid simulations, especially for the solid volume fraction. The coarse grid simulation predicts more dilute solid concentration in the dense region of the fluidized bed reactor and slight higher bed expansion height. The reason is that the internal meso-scale structure in a computational cell

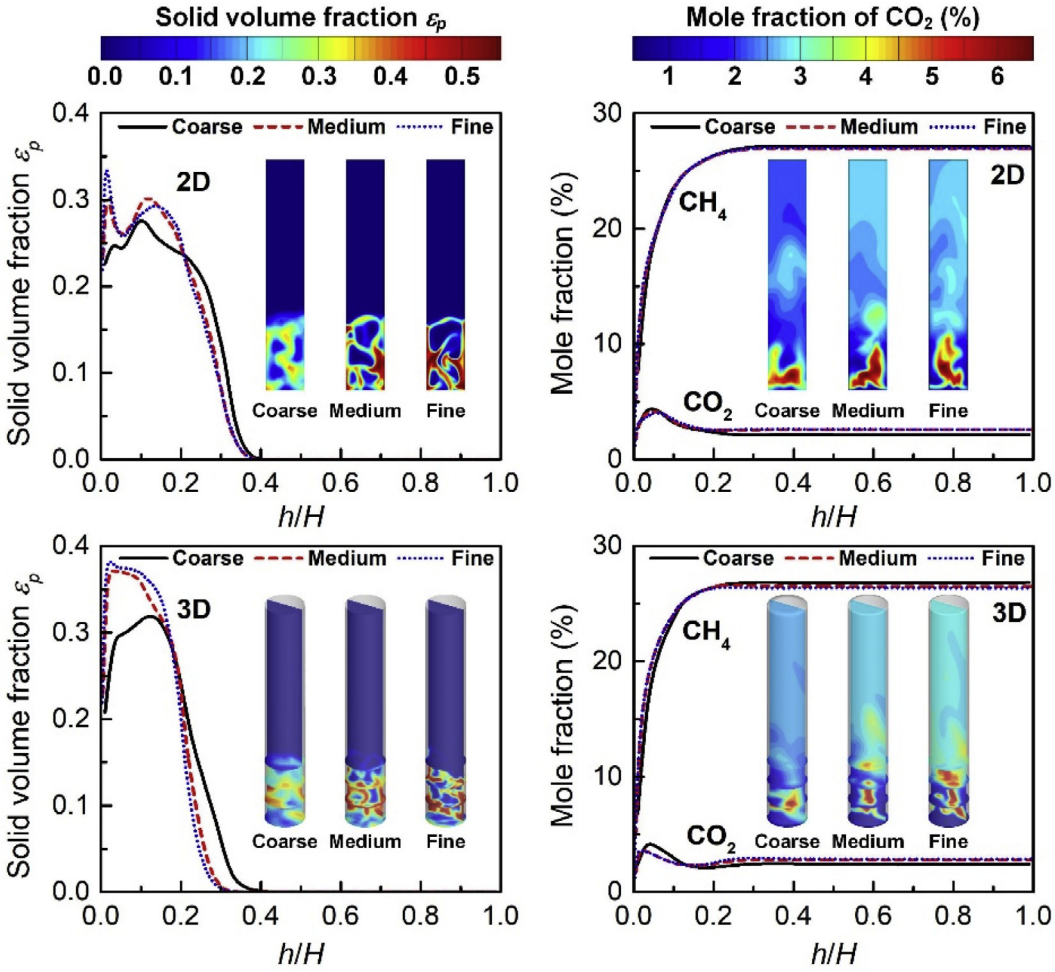

Fig. 3. Grid independence for the CFD model.

in coarse grid simulation cannot fully resolve, and thus the gas–solid drag force is still overestimated. Meanwhile, an ambiguous interface between the emulsion phase and bubble phase are obtained by the coarse grid simulation because the grid resolution is too low to capture the detail flow structure. A slight lower CO_2 mole fraction and higher CH_4 mole fraction at the outlet of the reactor are given by the coarse grid CFD simulation because of the numerical diffusion, while those obtained by the medium and fine grid simulations are almost the same. Therefore, by considering both numerical accuracy and computational cost, the medium grid (grid size = 0.75 mm) is chosen in the following simulations.

4.2. Model validation

The simulation results are compared with a series of experimental data under various operating conditions including temperature, inlet composition, inlet velocity and initial bed height to validate the reliability of the multi-scale CFD model, as shown in Fig. 4. The coefficient of determination (r^2) is adopted to characterize the adjacent degrees between the simulation results and experimental data.

$$r^2 = 1 - \frac{\sum_i (y_i^{\text{Exp.}} - y_i^{\text{Sim.}})^2}{\sum_i (y_i^{\text{Exp.}} - \bar{y}_i^{\text{Exp.}})^2}$$

It can be observed from the figures that, in general, the simulation results are in good agreement with the experimental data ($r^2 > 0.93$ for all the cases), which indicates that the the multi-scale model can be accurately applied to simulate the fluidized bed methanation process. However, the predictions of the H_2 mole fraction always have relative larger deviation than those of other species. The reason can be attributed to two aspects. On the one hand, H_2 has small mole weight of $2\ \text{g·mol}^{-1}$; this leads to that the mole fraction of H_2 is more sensitive, which means a small error in the mass fraction of H_2 can cause a significant deviation in the mole fraction. In addition, the mole fraction of H_2 is also sensitive to that of CO and CO_2. In CO methanation reaction, one mole consumption of CO will result in three moles consumption of H_2; in water–gas shift reaction, one mole consumption of CO_2 will result in one mole consumption of H_2 and one mole generation of CO, and then the CO will continue leading to three moles consumption of H_2 because the CO methanation reaction has large equilibrium constant in the temperature range of this study. Therefore, small prediction errors of CO and CO_2 can result in larger prediction error of H_2. Moreover, it can also be found from Fig. 4 that the 3D simulations provide better predictions ($r^2 > 0.95$) than 2D simulations. 3D simulations can accurately reflect the reality of the experimental apparatus while the 2D simulations are based on more approximations. Therefore, only 3D simulations are performed in the following sections in this paper.

4.3. Effects of chemical reactions on meso-scale structure

Cold flow CFD simulation (without chemical reactions) are

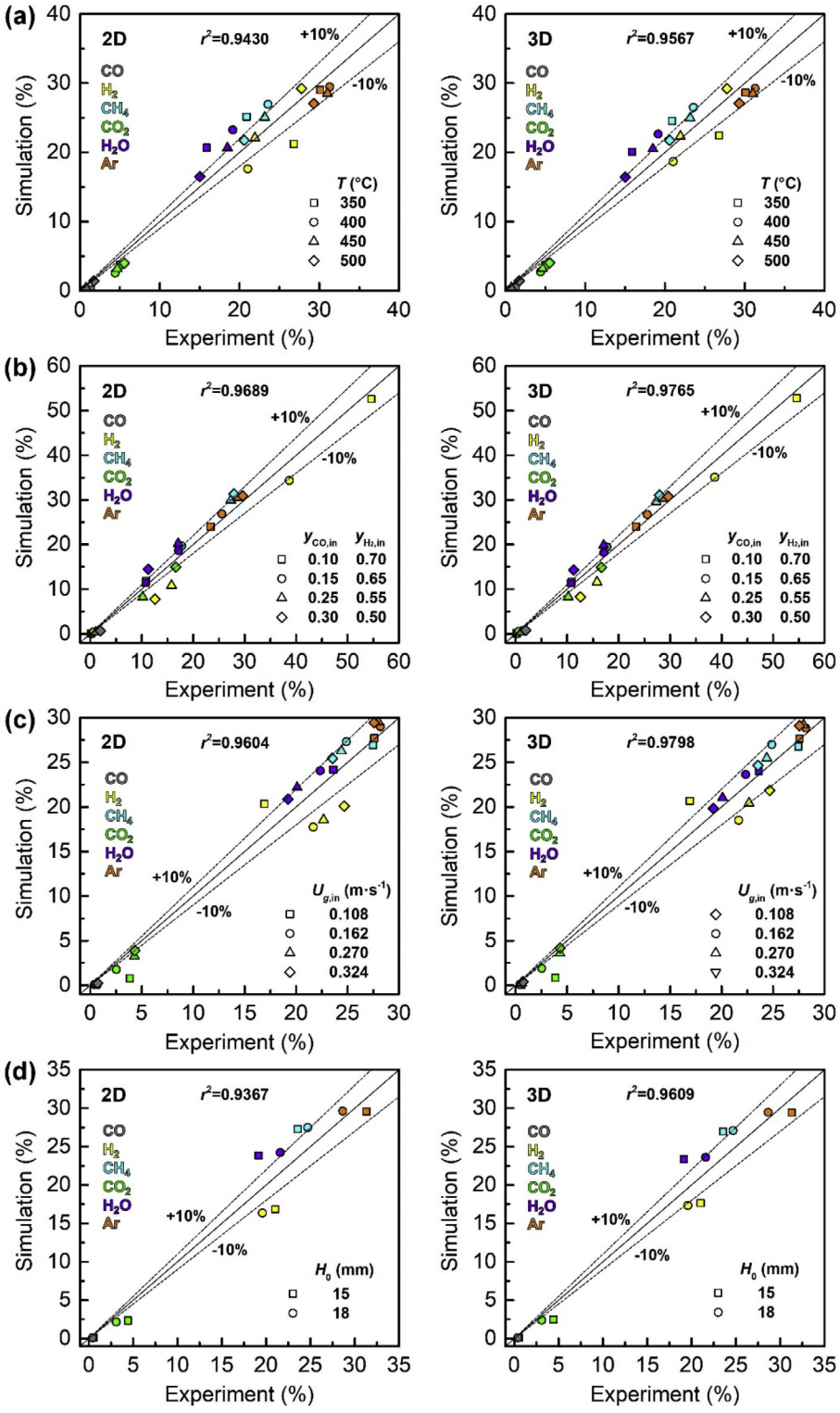

Fig. 4. Comparison of experimental data and simulation results at (a) different temperatures, (b) different inlet compositions, (c) different inlet velocities and (d) different initial bed heights.

performed to demonstrate the effects of chemical reactions on the mesoscale structure in the fluidized bed methanation process. Fig. 5 shows the contours of time-averaged solid volume fraction (ε_p) and axial gas velocity ($u_{g,\mathrm{axial}}$) obtained by cold flow and reactive flow simulations. It can be observed from the figure that the time-averaged axial gas velocity obtained by the cold flow simulations is much larger, and the time-averaged solid volume fraction is more dilute and the bed expansion height is slightly higher. By contrast, the time-averaged axial gas velocity in the reactive flow is much lower and the particle concentration is higher. The main reason for the difference between cold flow and reactive flow is that CO methanation, as the main reaction in the system, is characterized by the significant mole number reduction. Therefore, as the reactions proceed, the gas volume contracts and the gas velocity decreases. These changes in the reactor will further

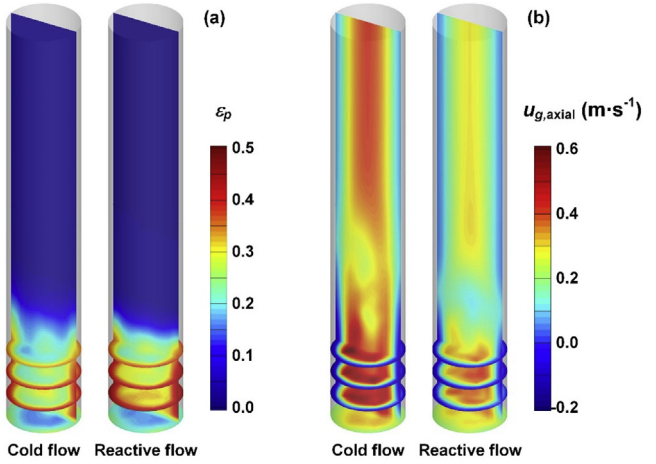

Fig. 5. Contours of time-averaged (a) solid volume fraction and (b) axial gas velocity ($T = 400$ °C, $y_{CO,in}$:$y_{H2,in}$:$y_{Ar,in} = 2$:6:2, $U_{g,in} = 0.216$ m·s^{-1} and $H_0 = 12$ mm).

influence the meso-scale structure.

In a bubbling fluidized bed, the meso-scale structure is characterized by the parameters of gas bubble (i.e. meso-scale structural parameters) such as bubble volume fraction (δ_b) and bubble velocity (U_{gb}). These meso-scale structural parameters can be calculated by the following approach from the CFD simulation results. The dense region ($h < H_{exp}$), determined by the pressure drop profile, for a transient result is equally divided into 20 layers in the axial direction. The overall voidage of each layer can be expressed as

$$\varepsilon_{g,overall} = \frac{1}{\sum V_{cell,i}} \sum (V_{cell,i} \cdot \varepsilon_{cell,i}) \tag{44}$$

where $V_{cell,i}$ and $\varepsilon_{cell,i}$ are volume and local voidage in ith computational cell, respectively. The bubble phase and emulsion phase are recognized by a threshold value of local voidage (0.7) in each layer. Then, the bubble volume fraction and bubble velocity can be obtained as

$$\delta_b = \frac{1}{\sum V_{cell,i}} \sum \left(V_{cell,i}|_{\varepsilon_{cell,i} > 0.7} \right) \tag{45}$$

$$u_{gb} = \frac{1}{\sum V_{cell,i}|_{\varepsilon_{cell,i} > 0.7}} \sum \left(V_{cell,i}|_{\varepsilon_{cell,i} > 0.7} \cdot u_{g,cell,i}|_{\varepsilon_{cell,i} > 0.7} \right) \tag{46}$$

where $u_{g,cell,i}$ is axial gas velocity in ith computational cell. Thus, the meso-scale structural parameters can be calculated by the CFD simulations. Meanwhile, these parameters can also be calculated by some correlations. In a cross-section of dense region in a fluidized bed reactor, the overall voidage and superficial gas velocity can be expressed as

$$\varepsilon_{g,overall} = (1-\delta_b)\varepsilon_e + \delta_b \varepsilon_b \tag{47}$$

$$U_g = (1-\delta_b)U_{ge} + \delta_b U_{gb} \tag{48}$$

where ε_e and ε_b are voidages in the emulsion phase and bubble phase, respectively. ε_e can be calculated using empirical correlation [25]

$$\varepsilon_e = 1 - \frac{0.58(1-\varepsilon_{g,overall})^{1.48}}{0.013 + (1-\varepsilon_{g,overall})^{1.48}} \tag{49}$$

ε_b is set as 0.9 here. U_{ge} is the gas velocity in the emulsion phase and is approximately equal to the minimum fluidization velocity (U_{mf}). Then, δ_b and U_{gb} can be obtained by the correlations.

Fig. 6 shows the meso-scale structural parameters as a function of the overall voidage obtained by CFD simulations and correlations under cold flow and reaction flow conditions. It can be seen that the meso-scale structural parameters calculated by the two methods are basically consistent and have the same trend, where δ_b increases linearly with $\varepsilon_{g,overall}$, and U_{gb} gradually decreases with $\varepsilon_{g,overall}$. From Fig. 6(a), it can be found that the δ_b obtained from the cold flow and the reaction flow do not seem to have a significant difference. In fact, the chemical reaction in the methanation system affects δ_b by reducing $\varepsilon_{g,overall}$. When the methanation reaction occurs, the volumetric shrinkage of the gas phase causes the superficial gas velocity to decrease, thereby reducing $\varepsilon_{g,overall}$, and thus δ_b also decreases. This can be seen from the probability density distribution of d_b, as shown in Fig. 7. In the cold flow, δ_b is concentrated in 0.3–0.6; in the reaction flow, the range reduces to 0.2–0.4. The effect of the chemical reactions on the bubble velocity can be clearly seen in Fig. 6(b). From this figure, the U_{gb} calculated from the reaction flow is obviously smaller than that obtained from the cold flow. The reason is the gas volume contraction due to chemical reactions.

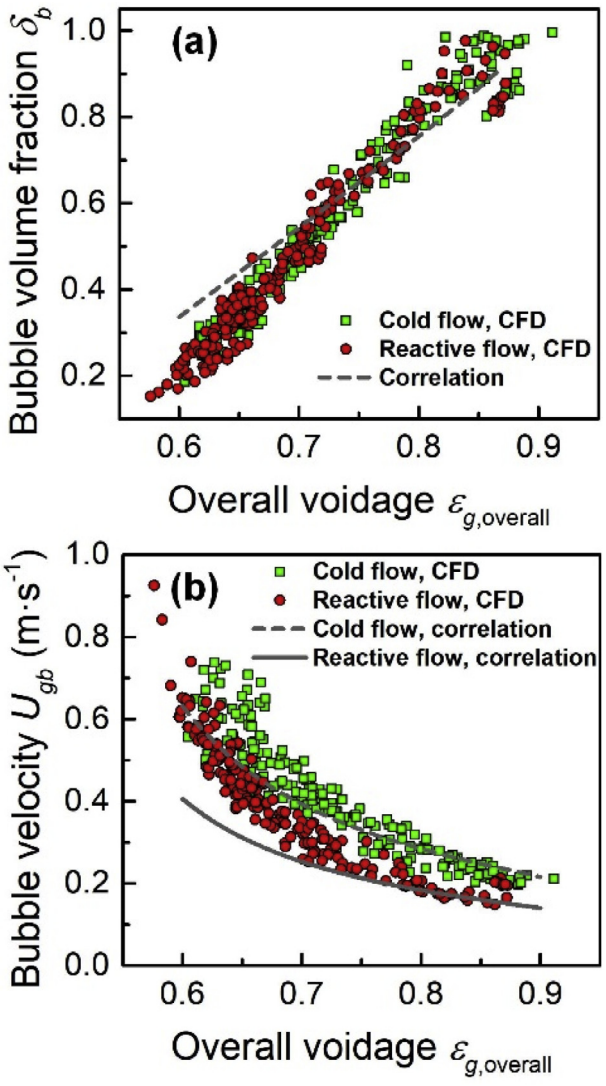

Fig. 6. Effects of chemical reactions on (a) bubble volume fraction and (b) bubble velocity.

4.4. Effects of energy equations (E-Eqs.) on the model results

The above simulation results are all based on the isothermal flow assumption (without solving the E-Eqs.). To verify the rationality of this

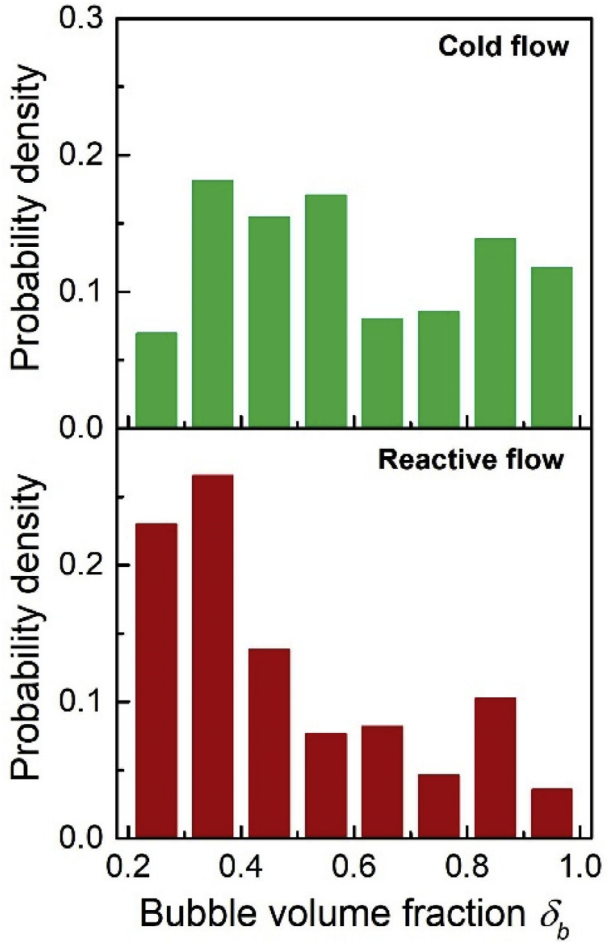

Fig. 7. Probability density distribution of the bubble volume fraction in cold flow and reactive flow.

hypothesis, this section will use operating conditions of $T = 400\,^{\circ}\mathrm{C}$, $y_{CO,in}$:$y_{H2,in}$:$y_{Ar,in}$ = 2:6:2, $U_{g,in} = 0.216\ \mathrm{m{\cdot}s^{-1}}$ and $H_0 = 12\ \mathrm{mm}$ as the reference case, and the E-Eqs. are solved under the same operating conditions as the reference case to investigate the influence of the E-Eqs. on the simulation results. In order to ensure the temperature at the outlet of the dense region of the fluidized bed reactor is approximately 400 °C, the thermal boundary condition of the wall is set to a fixed temperature of 391.7 °C, and the rest of the simulation settings remain unchanged. The results obtained will be discussed below.

Fig. 8 shows the distributions of the time-averaged gas temperature with solving the E-Eqs. According to the temperature distributions, the entire bed can be divided into three regions in axial direction: 1) hot spot temperature region ($h/H < 0.1$), 2) constant temperature region ($0.1 < h/H < 0.3$), and 3) freeboard region ($h/H > 0.3$). In the hot spot temperature region, since the methanation reaction is a highly exothermic reaction and has the fastest reaction rate, the gas temperature increase by approximately 18 °C after the gas enters the reactor. As the bed height increases, the thermodynamic limitation becomes more significant, the reaction rate therefore decreases, and thus the reaction heat release rate decreases. Under the combined effect of wall heat removal and reaction heat release, the gas temperature gradually decreases to approximately 400 °C. In the constant temperature region, due to the large heat capacity of the catalyst particles and the sufficient contacts and mixing of the particle-to-particle and the particle-to-gas, the temperature of this region is constant at about 400 °C. In the freeboard region, because there are almost no particles, the gas

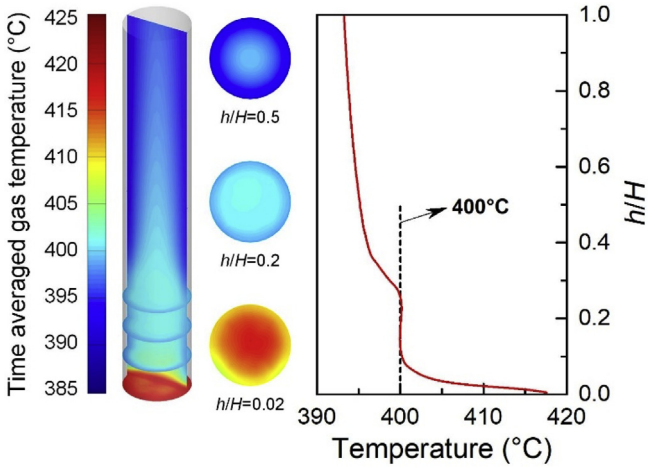

Fig. 8. Time-averaged gas temperature profile obtained by solving energy equations.

phase carrying a small amount of heat is rapidly cooled due to the heat removal from the wall, and the gas temperature eventually trends to the wall temperature.

From the analysis of Fig. 8 it can be found that there is a certain difference between the temperature distribution obtained by solving the E-Eqs. and that of the isothermal flow assumption. The effects of this difference on the simulation results should be evaluated. Fig. 9 shows the distributions of the solid volume fraction and the mole fraction of each species obtained by the CFD simulations with and without solving the E-Eqs. As can be seen in the figure, although there is a certain difference in the temperature distribution, the differences in the distributions of the solid volume fraction are not obvious. The main factor affecting the distribution of solid volume fraction is the superficial gas velocity, and the introduction of E-Eqs. does not have a significant effect on the superficial gas velocity. Therefore, the distribution of the solid volume fraction is almost the same. Chemical reaction rates and gas mixing are the main factors that affect the distribution of mole fractions. Although the change in temperature will cause a change in the chemical reaction rate, the gas mixing in the fluidized bed reactor is still more significant, resulting in almost no influence on the distribution of the mole fractions. As a results, the isothermal flow assumption is reasonable in the simulation of fluidized bed methanation if the temperature distribution in the reactor is not concerned.

5. Conclusion

Based on the Eulerian-Eulerian scheme with the kinetic theory of granular flow, a multi-scale CFD simulation method is proposed to numerically predict the fluidized bed methanation process. The governing equations in the macro-scale calculate the parameters of a computational cell, which is used as the input of the meso-scale and micro-scale models. An improved LSD drag model is adopted as the meso-scale model to close the gas and solid momentum equations in the macro-scale model. The micro-scale chemical reactions provide the reaction rates for the species transport equations and heat source for the energy equations in the macro-scale. This model results are consistent with the experimental data obtained in a lab-scale fluidized bed reactor under wide operating conditions. The results obtained by 3D simulations are more accurate than those obtained by 2D simulations.

The effects of the chemical reactions on the meso-scale structure and the effects of the energy equations on the model results are studied. Due to the mole number reduction of the methanation reaction, the superficial gas velocity decreases when the chemical reactions are

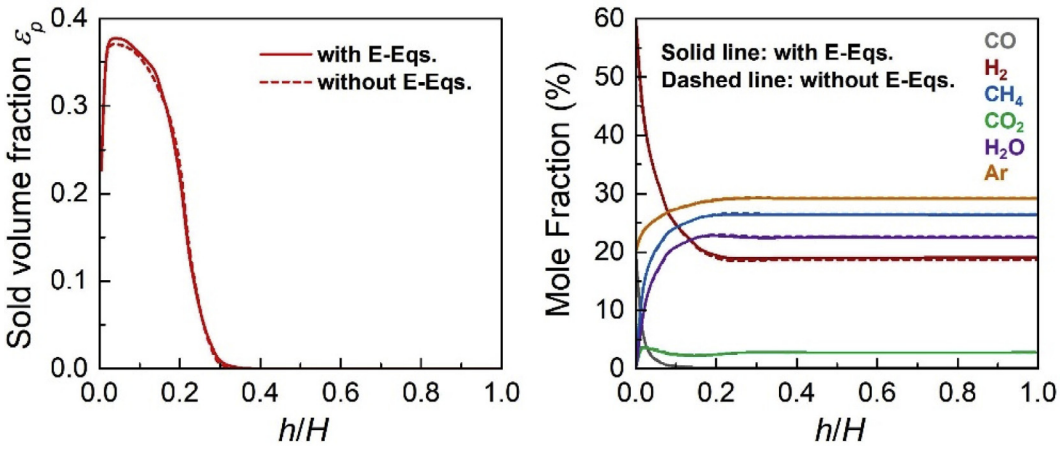

Fig. 9. Effects of energy equations on the distributions of solid volume fraction and mole fraction.

enabled, resulting in the decrease of bubble volume fraction and bubble velocity. When solving the model with the energy equations, the distribution of gas temperature can be divided into hot spot temperature region, constant temperature region and the freeboard region. However, the obtained distributions of solid volume fractions and the mole fractions nearly remain the same as the simulation results with the isothermal flow assumption.

Acknowledgement

This work was supported by the Major Research Plan of National Natural Science Foundation of China (No. 91334101).

References

[1] Q. Eri, J. Peng, X. Zhao, CFD simulation of biomass steam gasification in a fluidized bed based on a multi-composition multi-step kinetic model, Appl. Therm. Eng. 129 (2018) 1358–1368.
[2] L.M. Armstrong, S. Gu, K.H. Luo, Effects of limestone calcination on the gasification processes in a BFB coal gasifier, Chem. Eng. J. 168 (2011) 848–860.
[3] J. Kopyscinski, T.J. Schildhauer, S.M.A. Biollaz, Fluidized-bed methanation: interaction between kinetics and mass transfer, Ind. Eng. Chem. Res. 50 (2011) 2781–2790.
[4] S. Rönsch, J. Schneider, S. Matthischke, M. Schlüter, M. Götz, J. Lefebvre, P. Prabhakaran, S. Bajohr, Review on methanation—From fundamentals to current projects, Fuel 166 (2016) 276–296.
[5] I. Julián, J. Herguido, M. Menéndez, CFD model prediction of the two-section two-zone fluidized bed reactor (TS-TZFBR) hydrodynamics, Chem. Eng. J. 248 (2014) 352–362.
[6] S. Wang, H. Lu, F. Zhao, G. Liu, CFD studies of dual circulating fluidized bed reactors for chemical looping combustion processes, Chem. Eng. J. 236 (2014) 121–130.
[7] J. Li, M. Kwauk, Exploring complex systems in chemical engineering—the multi-scale methodology, Chem. Eng. Sci. 58 (2003) 521–535.
[8] J. Li, W. Ge, J. Zhang, M. Kwauk, Multi-scale compromise and multi-level correlation in complex systems, Chem. Eng. Res. Des. 83 (2005) 574–582.
[9] J. Li, J. Zhang, W. Ge, X. Liu, Multi-scale methodology for complex systems, Chem. Eng. Sci. 59 (2004) 1687–1700.
[10] Z. Shi, W. Wang, J. Li, A bubble-based EMMS model for gas-solid bubbling fluidization, Chem. Eng. Sci. 66 (2011) 5541–5555.
[11] K. Hong, Z. Shi, W. Wang, J. Li, A structure-dependent multi-fluid model (SFM) for heterogeneous gas-solid flow, Chem. Eng. Sci. 99 (2013) 191–202.
[12] J. Li, X. Tian, B. Yang, Hydromechanical simulation of a bubbling fluidized bed using an extended bubble-based EMMS model, Powder Technol. 313 (2017) 369–381.
[13] S.K. Kanholy, B. Estejab, F. Battaglia, Modeling multiple gas jet interactions during fluidization in a pseudo-2D bed, Chem. Eng. J. 328 (2017) 1009–1021.
[14] N. Yang, W. Wang, W. Ge, L. Wang, J. Li, Simulation of heterogeneous structure in a circulating fluidized-bed riser by combining the two-fluid model with the EMMS approach, Ind. Eng. Chem. Res. 43 (2004) 5548–5561.
[15] K. Agrawal, P.N. Loezos, M. Syamlal, S. Sundaresan, The role of meso-scale structures in rapid gas-solid flows, J. Fluid Mech. 445 (2001).
[16] Y. Zhao, H. Li, M. Ye, Z. Liu, 3D numerical simulation of a large scale MTO fluidized bed reactor, Ind. Eng. Chem. Res. 52 (2013) 11354–11364.
[17] M. Salehi, M. Askarishahi, H.R. Godini, R. Schomäcker, G. Wozny, CFD simulation of oxidative coupling of methane in fluidized-bed reactors: a detailed analysis of flow-reaction characteristics and operating conditions, Ind. Eng. Chem. Res. 55 (2016) 1149–1163.
[18] Y. Liu, O. Hinrichsen, CFD simulation of hydrodynamics and methanation reactions in a fluidized-bed reactor for the production of synthetic natural gas, Ind. Eng. Chem. Res. 53 (2014) 9348–9356.
[19] L. Sun, K. Luo, J. Fan, Numerical simulation of CO methanation for the production of synthetic natural gas in a fluidized bed reactor, Energ. Fuel. 31 (2017) 10267–10273.
[20] J. Kopyscinski, T.J. Schildhauer, F. Vogel, S.M.A. Biollaz, A. Wokaun, Applying spatially resolved concentration and temperature measurements in a catalytic plate reactor for the kinetic study of CO methanation, J. Catal. 271 (2010) 262–279.
[21] J. Li, B. Yang, CFD simulation of bubbling fluidized beds using a local-structure-dependent drag model, Chem. Eng. J. 329 (2017) 100–115.
[22] D.J. Gunn, Transfer of heat or mass to particles in fixed and fluidized beds, Int. J. Heat Mass Transfer 21 (1978) 467–476.
[23] J. Kopyscinski, T.J. Schildhauer, S.M.A. Biollaz, Methanation in a fluidized bed reactor with high initial CO partial pressure: Part II—Modeling and sensitivity study, Chem. Eng. Sci. 66 (2011) 1612–1621.
[24] J. Li, B. Yang, Bubbling fluidized bed methanation study with resolving the meso-scale structure effects. Submitted, 2018.
[25] A.T. Harris, J.F. Davidson, R.B. Thorpe, The prediction of particle cluster properties in the near wall region of a vertical riser (200157), 127 (2002) 128–143.